Conservative discretization of Poisson's equation on locally refined grids and its solution method by multigrid (Discretization Methods and Numerical Algorithms for Differential Equations)

AUTHOR(S):

Washio, Takumi

CITATION:

Washio, Takumi. Conservative discretization of Poisson's equation on locally refined grids and its solution method by multigrid (Discretization Methods and Numerical Algorithms for Differential Equations). 数理解析研究所講究録 2002, 1265: 107-117

ISSUE DATE:

2002-05

URL:

http://hdl.handle.net/2433/42079

数理解析研究所講究録 1265 巻 2002 年 107-117

Conservative discretization of Poisson's equation on locally refined grids and its solution method by multigrid

日本電気 (株) 基礎研究所 鷲尾 巧 (T. Washio)
Fundamental Research Laboratories, NEC Corporation, 1-1, Miyazaki 4-chome, Miyamae-ku, Kawasaki, Kanagawa 216-8555, Japan (email: t-washio@bk.jp.nec.com)

1 Introduction

In this article, three dimensional conservative discretization methods of Poisson's equation:

$$-\Delta u = g \tag{1}$$

on composite cells and its solution method by multigrid are introduced. Needs of such a solver arise in computation of electrostatic potential for a variety of applications which deal with infinite spaces or source terms of locally concentrated charge distributions. The conservative discretizations considered here are for the second and the fourth order accuracy. The fourth order accuracy is achieved by so called Mehrstellen discretization [5, 4]. By this compact discretization scheme, much more accurate solution than that by the standard second order discretization can be obtained even on relatively coarse grids. The discretization considered here is a cell centered discretization on composite cells, where unknowns are located at the cell centers. The composite cells cover the domain without any space at the fine-coarse interfaces like the two dimensional image in Fig. 1. The conservation is achieved by the idea introduced by Brandt and Bai[1, 2]. Here, a clear view for the conservation technique is given by explicitly showing flux balance at each cell around the fine-coarse cell interface.

Next, a solution method by multigrid for the conservative discretizations is also described. This can be achieved with slight modification of the standard MLAT (Multilevel Adaptive Technique) approach due to Brandt[3].

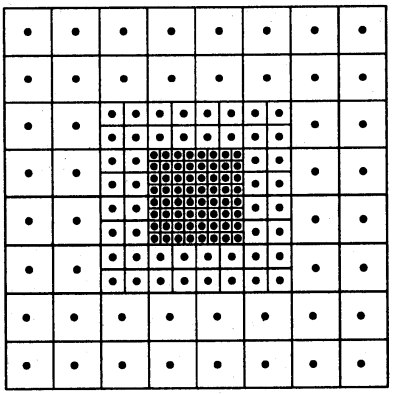

Figure 1: Composite cells and their central points where unknowns are located.

2 A higher order flux approximation

In this section, an interpretation of a fourth order discretization as a finite volume discretization is given. The fourth-order accuracy can be achieved with a 3D Mehrstellen discretization:

$$-\Delta_h^M u_h = R_h^M g_h, \tag{2}$$

where Δ_h^M is the compact 19-points stencil and R_h^M is the 7-points stencil:

$$-\Delta_h^M = \frac{1}{6h^2}\left[\begin{bmatrix} 0 & -1 & 0 \\ -1 & -2 & -1 \\ 0 & -1 & 0 \end{bmatrix}_h \begin{bmatrix} -1 & -2 & -1 \\ -2 & 24 & -2 \\ -1 & -2 & -1 \end{bmatrix}_h \begin{bmatrix} 0 & -1 & 0 \\ -1 & -2 & -1 \\ 0 & -1 & 0 \end{bmatrix}_h\right]_h, \tag{3}$$

$$R_h^M = \frac{1}{12}\left[\begin{bmatrix} 0 & 0 & 0 \\ 0 & 1 & 0 \\ 0 & 0 & 0 \end{bmatrix}_h \begin{bmatrix} 0 & 1 & 0 \\ 1 & 6 & 1 \\ 0 & 1 & 0 \end{bmatrix}_h \begin{bmatrix} 0 & 0 & 0 \\ 0 & 1 & 0 \\ 0 & 0 & 0 \end{bmatrix}_h\right]_h. \tag{4}$$

It can be easily verified by Taylor's expansion of u and g that this discretization is $O(h^4)$. The 3D Mehrstellen discretization can be interpreted as a finite volume discretization due to the following flux approximation.

Lemma 2.1 *Under an appropriate smoothness assumption on u, the flux for ∇u from a xy-cell face with size h can be approximated as follows.*

$$\begin{aligned}&\frac{1}{h^2}\int_{-\frac{h}{2}}^{\frac{h}{2}}\int_{-\frac{h}{2}}^{\frac{h}{2}} u_z(x,y,\frac{h}{2})dxdy \\ &\quad = \frac{1}{12h}\left[\begin{bmatrix} 0 & 1 & 0 \\ 1 & 8 & 1 \\ 0 & 1 & 0 \end{bmatrix}_h \begin{bmatrix} 0 & -1 & 0 \\ -1 & -8 & -1 \\ 0 & -1 & 0 \end{bmatrix}_h\right]_h u + \frac{h}{24}(g_{00h} - g_{000}) + O(h^4).\end{aligned} \tag{5}$$

Proof
First, note that the following approximation holds for the integral of a 2D smooth function f on a square with size h.

$$\frac{1}{h^2}\int_{-\frac{h}{2}}^{\frac{h}{2}}\int_{-\frac{h}{2}}^{\frac{h}{2}} f(x,y)dxdy = \frac{1}{6}\begin{bmatrix} 0 & 1 & 0 \\ 1 & 2 & 1 \\ 0 & 1 & 0 \end{bmatrix}_{\frac{h}{2}} f + O(h^4). \tag{6}$$

The above approximation is obtained from Taylor's expansion of f at the origin, where the odd order terms in one direction like xy, x^3, x^2y, xy^2, y^3 are canceled out due to their antisymmetry. Our aim for introducing (6) is to apply it to u_z in an upper xy-cell face. u_z can be approximated at the sampled points as follows. Here, the indices attached to functions are represented without the factor h for simplicity.

$$\begin{aligned}u_{z,00\frac{1}{2}} &= \frac{u_{001} - u_{000}}{h} - \frac{1}{24}u_{zzz,00\frac{1}{2}}h^2 + O(h^4), \\ u_{z,0-\frac{1}{2}\frac{1}{2}} &= \frac{u_{0-11} + u_{001} - u_{0-10} - u_{000}}{2h} - \frac{1}{8}u_{yyz,0-\frac{1}{2}\frac{1}{2}}h^2 - \frac{1}{24}u_{zzz,0-\frac{1}{2}\frac{1}{2}}h^2 + O(h^4), \\ u_{z,-\frac{1}{2}0\frac{1}{2}} &= \frac{u_{-101} + u_{001} - u_{-100} - u_{000}}{2h} - \frac{1}{8}u_{xxz,-\frac{1}{2}0\frac{1}{2}}h^2 - \frac{1}{24}u_{zzz,-\frac{1}{2}0\frac{1}{2}}h^2 + O(h^4),\end{aligned}$$

$$u_{z,\frac{1}{2}0\frac{1}{2}} = \frac{u_{101}+u_{001}-u_{100}-u_{000}}{2h} - \frac{1}{8}u_{xxz,\frac{1}{2}0\frac{1}{2}}h^2 - \frac{1}{24}u_{zzz,\frac{1}{2}0\frac{1}{2}}h^2 + O(h^4),$$
$$u_{z,0\frac{1}{2}\frac{1}{2}} = \frac{u_{011}+u_{001}-u_{010}-u_{000}}{2h} - \frac{1}{8}u_{yyz,0\frac{1}{2}\frac{1}{2}}h^2 - \frac{1}{24}u_{zzz,0\frac{1}{2}\frac{1}{2}}h^2 + O(h^4).$$

Thus the flux per unit area from the upper xy-cell face is given by

$$\begin{aligned}
\frac{1}{h^2}\int_{-\frac{h}{2}}^{\frac{h}{2}}\int_{-\frac{h}{2}}^{\frac{h}{2}} u_z(x,y,\frac{h}{2})dxdy &= \frac{1}{6}\begin{bmatrix}0&1&0\\1&2&1\\0&1&0\end{bmatrix}_{\frac{h}{2}} u_{z,**\frac{h}{2}} + O(h^4) \\
&= \frac{1}{12h}\left[\begin{bmatrix}0&1&0\\1&8&1\\0&1&0\end{bmatrix}_h \begin{bmatrix}0&-1&0\\-1&-8&-1\\0&-1&0\end{bmatrix}_h\right]_h u - \frac{h^2}{48}\begin{bmatrix}0&0&0\\1&0&1\\0&0&0\end{bmatrix}_h u_{xxz,*,*,\frac{1}{2}} \\
&\quad - \frac{h^2}{48}\begin{bmatrix}0&1&0\\0&0&0\\0&1&0\end{bmatrix}_h u_{yyz,*,*,\frac{1}{2}} - \frac{h^2}{144}\begin{bmatrix}0&1&0\\1&2&1\\0&1&0\end{bmatrix}_h u_{zzz,*,*,\frac{1}{2}} + O(h^4) \\
&= \frac{1}{12h}\left[\begin{bmatrix}0&1&0\\1&8&1\\0&1&0\end{bmatrix}_h \begin{bmatrix}0&-1&0\\-1&-8&-1\\0&-1&0\end{bmatrix}_h\right]_h u \\
&\quad - \frac{h^2}{24}(u_{xxz,00\frac{1}{2}} + u_{yyz,00\frac{1}{2}} + u_{zzz,00\frac{1}{2}}) + O(h^4)
\end{aligned}$$

This leads to (5). ■

Note that the approximation (5) is a higher order version of the standard second order approximation:

$$\frac{1}{h^2}\int_{-\frac{h}{2}}^{\frac{h}{2}}\int_{-\frac{h}{2}}^{\frac{h}{2}} u_z(x,y,\frac{h}{2})dxdy = \frac{1}{h}(u_{001}-u_{000}) + O(h^2). \tag{7}$$

3 Flux conservation at the fine-coarse cell interface

The discretization of Poisson's equation is given as in the equidistant grid case for the internal cells that are not adjacent to cells of a different size. For discussions of the discretization at the fine-coarse cell interfaces, let us define six sets of cells with size h according to their positions as follows (See the two dimensional image in Fig. 2).

C_h^{r} : The real cells in the composite cells with size h
C_h^{rf}: The real cells in the layer adjacent to the finer cell with size $h/2$
C_h^{rc}: The real cells in the layer adjacent to the coarser cell with size $2h$
C_h^{gi}: The ghost cells inside C_h^{r}
C_h^{go}: The ghost cells in the layer just outside C_h
C_h : $C_h^{\mathrm{r}} \cup C_h^{\mathrm{gi}} \cup C_h^{\mathrm{go}}$

For the cells in C_h^{rc} and C_H^{rf} $(H = 2h)$, the discretization can be given once function values on the ghost cells C_h^{go} and C_H^{gi} are given by appropriate interpolations. However, such a discretization leads to the inconsistency of the fluxes at the fine-coarse cell interfaces. Thus, the

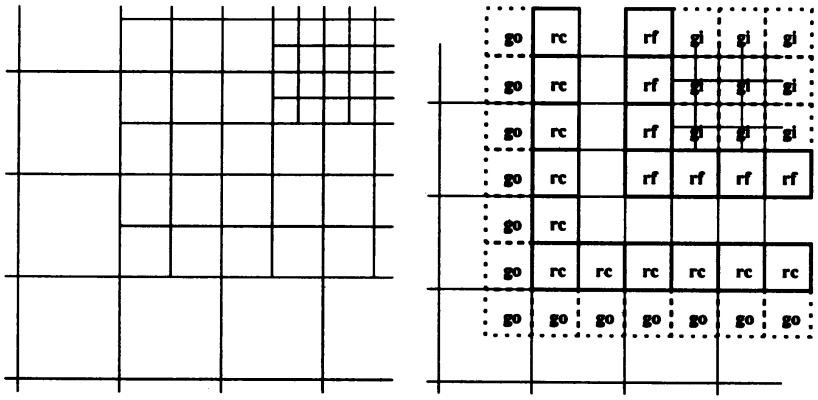

Figure 2: Composite cells at the corner in (a). The two layers of the real cells (C_h^{rf} and C_h^{rc}) and the two sets of the ghost cells (C_h^{gi} and C_h^{go}) in (b).

flux is not preserved. The consistency is regained by adjusting the flux into the coarse cell by sum of the fluxes from the four fine cells adjacent to the coarser cell. For example, in case of the xy fine-coarse cell interface where the lower side of the coarse cell is adjacent to the upper side of the fine cells (See Fig. 3), the conservative discretization ($\check{\Delta}$) can be given as follows.

$$-\check{\Delta}_h \mathcal{U} := -\Delta_h u_h, \text{ at } c_h(k)\ (k = 1,2,3,4), \tag{8}$$

$$-\check{\Delta}_H \mathcal{U} := -\Delta_H u_H - \frac{1}{H}\nabla_{z,H} u_H \text{ on } f_{xy}^{-}(c_H) + \frac{1}{4H}\sum_{k=1}^{4} \nabla_{z,h} u_h \text{ on } f_{xy}^{+}(c_h(k)), \text{ at } c_H. \tag{9}$$

Here, u_h and u_H represent the function values, respectively, on C_h and on C_H, where the values on the ghost cells are assumed to be given with the interpolations. $\mathcal{U}$ at the left hand side mean the values on the composite cells. Note that each of the interpolations on C_h^{go} and on C_H^{gi} is accomplished by referring not only the function values on individual level but with on the two levels. Therefore, such the notation $\mathcal{U}$ is introduced here. The notations $\nabla_{z,H}$ and $\nabla_{z,h}$ mean the discretized flux (5) or (7) along the z-direction per xy-unit area on the coarse cell face and on the fine cell face, respectively. $f_{xy}^{-}(c_H)$ represents the xy-cell face at the bottom of c_H, which is adjacent to the four fine cells below. $f_{xy}^{+}(c_h(k))(k = 1,2,3,4)$ represent the cell faces at the upper side of these four fine cells.

4 The MLAT algorithm for the conservative discretization

The solution of the conservative discretization on the composite cells can be obtained by the MLAT (Multilevel Adaptive Technique) approach due to Brandt[3] with a slight modification of the right hand side at each level. The modification of the right hand side is based on a defect correction technique where the solution is updated according to the following equation.

$$-\Delta_H u_{H,\mathbf{new}} = g_H + \check{\Delta}_H \mathcal{U}_{\mathbf{old}} - \Delta_H u_{H,\mathbf{old}}, \text{ at } c_H \in C_H^{\mathrm{r}}. \tag{10}$$

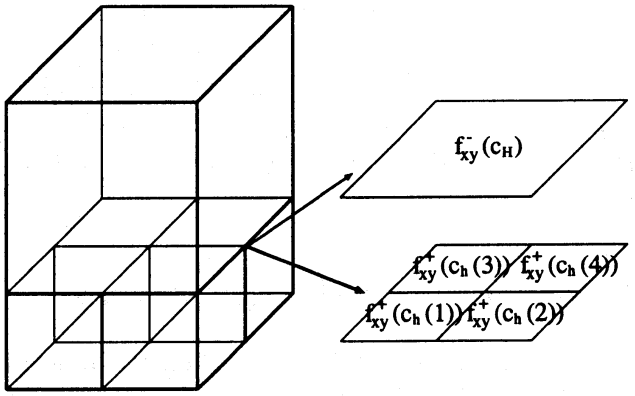

Figure 3: The xy fine-coarse interface.

Namely, the new values $u_{H,\mathbf{new}}$ on C^{r}_H are obtained just by updating them with the modified right hand side given from the old values $\mathcal{U}_{\mathbf{old}}$.

In the standard MLAT algorithm, the right hand side of the equation on the coarse cell C_H is constructed due to the FAS (Full Approximation Scheme) [3, 5] as follows.

$$\tilde{g}_H := \begin{cases} -\Delta_H \tilde{u}_H + r_H & \text{on } C^{\mathrm{gi}}_H \\ g_H & \text{on } C^{\mathrm{r}}_H \end{cases} \tag{11}$$

Here, $\tilde{u}_H$ is the initial guess on C^{gi}_H interpolated from the solution on $C_h \cup C^{\mathrm{r}}_H$. r_H is the residuals restricted on C^{gi}_H from C_h. If the conservation is taken into account, Equation (10) is incorporated in its construction as follows.

$$\tilde{g}_H := \begin{cases} -\Delta_H \tilde{u}_h + r_H & \text{on } C^{\mathrm{gi}}_H \\ g_H + \check{\Delta}_H \mathcal{U} - \Delta_H u_H & \text{on } C^{\mathrm{rf}}_H \\ g_H & \text{on } C^{\mathrm{r}}_H \backslash C^{\mathrm{rf}}_H \end{cases} \tag{12}$$

Here, the values on C^{rf}_H are given based on (10).
With the determination of the right hand side on the coarse grids either by (11) or (12), the two level MLAT algorithm is given as follows.

(Op1)	Interpolation on C^{go}_h	$u^{\mathrm{go}}_h := INTP^{\mathrm{go}}_h(u^{\mathrm{r}}_h, u^{\mathrm{r}}_H)$;
(Op2)	Pre-smoothing	$u_h := RELAX(u_h, \tilde{g}_h)$;
(Op3)	Computation of residuals	$r_h := \tilde{g}_h + \Delta_h u_h$;
(Op4)	Restriction of residuals	$r^{\mathrm{gi}}_H := I^H_h r_h$;
(Op5)	Interpolation on C^{gi}_H	$u^{\mathrm{rf}}_H := INTP^{\mathrm{gi}}_H(u^{\mathrm{r}}_h, u^{\mathrm{r}}_H)$;
(Op6)	Saving initial guess on C_H	$\tilde{u}_H := u_H$;
(Op7)	Solution on C_H	$-\check{\Delta}_H \mathcal{U} = \tilde{g}_H$ from (11) or (12);
(Op8)	Correction	$u_h := u_h + I^h_H(u_H - \tilde{u}_H)$;
(Op9)	Interpolation on C^{go}_h	$u^{\mathrm{go}}_h := INTP^{\mathrm{go}}_h(u^{\mathrm{r}}_h, u^{\mathrm{r}}_H)$;
(Op10)	Post-smoothing	$u_h := RELAX(u_h, \tilde{g}_h)$;

Note that $\tilde{g}_h$ is set with g_h on the finest grid. For the restriction I^H_h in (Op4), just the averaging of the residuals on the eight cells which comprise the coarse cell can be used. For the prolongation I^h_H in (Op8), the trilinear interpolation with the eight adjacent coarse cell points

can be applied. Also for the interpolation in (Op5) on the coarse cells in C_H^{gi}, the averaging of unknown on the eight adjacent fine cell points can be used except for the outermost cells.
Note that there is no relation between the quality of the discretization and the choice of these operations. However, the interpolations on the ghost cells on C_h^{go} and the outermost cells in C_H^{gi} have influence on the accuracy of solutions. In the next section, these operators will be introduced.

5 Interpolation operators on the ghost cells

In usual MLAT algorithm, a cubic interpolation is applied to determine the fine grid exterior boundary values for the second order discretization, since the second order truncation error for the Laplace operator is assured with it. As a natural extension of this idea, a fifth order interpolation should be applied in the fourth order discretization case.

Basically, interpolations here are constructed based on the one dimensional Lagrange interpolation where the weights w_i at a point x to the sampling points $\{x_1, x_2, \cdots, x_n\}$ are given by

$$w_i(x) = \prod_{j=1}^{i-1} \frac{x - x_j}{x_i - x_j} \prod_{j=i+1}^{n} \frac{x - x_j}{x_i - x_j}, \ 1 \leq i \leq n. \tag{13}$$

In multidimensional cases, interpolations are performed in the multiplicative manner from one dimension to other dimensions.

Let us start with the interpolations on the ghost cells at the exterior boundaries of the fine cells (C_h^{go}). The construction of the interpolation is shown here in the two dimensional case for the sake of simplicity. There are no difficulties to extend the idea to the three dimensional case. Let us consider the fifth order interpolation. As shown in Fig. 4 (a), the fifth order interpolations along the x-direction are performed for three coarse cell layers above the top and under the bottom of the fine cell box. After this, the fifth order interpolations on C_h^{go} along the y-direction where the six values on the three fine and the three coarse cells are sampled are performed. The same procedure is applied for the left and right hand boundaries of the fine cells. Note that the values on the corners in C_h^{go} can be also given in the latter interpolations by sampling the values obtained in the former interpolations. These values are necessary for the Mehrstellen discretization. The cubic order interpolations can be accomplished in a similar manner. Similarly, the interpolations at the interior boundaries of the coarse cells can be given as depicted in Fig. 4 (b). For example, in the case of the fifth order interpolation, the fifth order interpolation along the x-direction is performed on three fine cell layers at each of the top and the bottom of the fine cell box assuming that the ghost cell values at the exterior fine cell boundaries are given due to the interpolation introduced above. Then, the fifth order interpolation along the y-direction where the three fine cell values and the three coarse cell values are sampled takes place. Note that at least three (resp. two) layers must be present in the real cells at each level for the fifth (resp. cubic) order interpolation.

6 Cell configuration and its relation to the solution error

In [6], the relation between the L_∞ norm and the composite grid configuration is analyzed assuming that the support of the source term is contained in the finest grid. The analysis relies

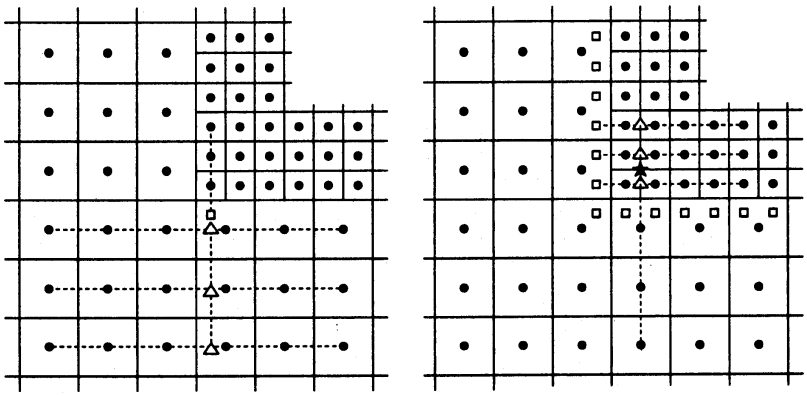

Figure 4: (a)The multidimensional fifth order interpolation on the exterior fine cell boundaries. First, the values on △ are computed by the fifth order interpolation along the x-direction. Then, the value on □ is interpolated from the three fine cell values and the three coarse cell values. (b)The multidimensional fifth order interpolation on the interior coarse cell boundaries. First, the values on △ are computed in the fifth order interpolation along the x-direction. Then, the value on ⋆ is interpolated from the three fine cell values and the three coarse cell values.

on the following estimate, which is likely satisfied under the conservative discretization.

$$|e(\mathbf{p})| \leq c \int \frac{\mathrm{trun}(\mathbf{r})}{G(\mathbf{r},\mathbf{p})} dr. \tag{14}$$

Here, $e(\mathbf{r})$ and $\mathrm{trun}(\mathbf{r})$ indicate the solution error at a point $\mathbf{r}$ and the truncation error at a point $\mathbf{r}$, respectively, and G is the Green function. For a point $\mathbf{r}$ apart from the concentration of the source term around the origin, the truncation error may be estimated like

$$|\mathrm{trun}_2(\mathbf{r})| \leq c\frac{h(\mathbf{r})^2}{|\mathbf{r}|^5}, \tag{15}$$

$$|\mathrm{trun}_4(\mathbf{r})| \leq c\frac{h(\mathbf{r})^4}{|\mathbf{r}|^7}, \tag{16}$$

where trun_2 and trun_4 indicate the truncation errors of the second and the fourth order discretizations, respectively, and $h(\mathbf{r})$ is the cell size at a point $\mathbf{r}$. As in [6], the composite cells here are constructed in the following manner (See Fig. 5).

First, we put the finest cell box around the concentrated part of the source term. Then, the coarser cell box which have the same center as that of the finest grid is extended by $\alpha(>1)$ times. The same procedures are done until the cell box covers sufficiently large domain. The parameter α is called the grid extension rate. From substituting (15) and (16) to (14), the following relations between the solution errors and the grid extension rate are derived.

$$|e_2| \leq c_1 {h_0}^2 + c_2 \sum_{k\geq 1} \left(\frac{2^2}{\alpha^3}\right)^k {h_0}^2, \tag{17}$$

$$|e_4| \leq c_1 {h_0}^4 + c_2 \sum_{k\geq 1} \left(\frac{2^4}{\alpha^5}\right)^k {h_0}^4. \tag{18}$$

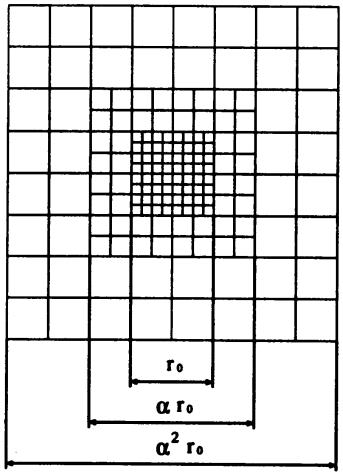

Figure 5: A cell configuration with three levels by the grid extension rate α.

Here, e_2 and e_4 indicate the solution errors for the second and the fourth order discretizations, respectively, and h_0 is the finest cell size. The first terms in these estimates originate in the truncation errors around the finest grid, and they are out of our focus here. These estimates mean that the grid extension rate must fulfill

$$\alpha < 2^{\frac{2}{3}} = 1.58\ldots \tag{20}$$

for the second order discretization, and

$$\alpha < 2^{\frac{4}{5}} = 1.74\ldots \tag{21}$$

for the fourth order discretization. Note that the grid extension rate affect the computational cost. In particular, the cost per one multigrid cycle is estimated like

$$\text{cost/cycle} \propto \sharp\{c_{h_0}\} \sum_{k \geq 1} \left(\frac{\alpha}{2}\right)^{3k}, \tag{22}$$

where $\sharp\{c_{h_0}\}$ is the total number of the finest cells.

7 Numerical experiments

In this section, we examine effects of the conservation technique on the accuracy of the solutions and on the computational costs of the multigrid solution method. Two different cases are investigated. One is a case where the support of the source term g is contained in the finest grid. In the other case, the source term decrease asymptotically as $e^{-|\mathbf{r}|}$ like electron density of insulated molecules.

Problem 1

$$g(\mathbf{r}) = \begin{cases} (1 - |\mathbf{r} - \mathbf{r_0}|^2)^4, & |\mathbf{r} - \mathbf{r_0}| \leq 1, \\ 0, & |\mathbf{r} - \mathbf{r_0}| > 1. \end{cases} \tag{23}$$

Problem 2

$$g(\mathbf{r}) = e^{-|\mathbf{r} - \mathbf{r_0}|}. \tag{24}$$

First, we will examine the relation between the solution error and the grid extension rate from the results in Problem 1. Here, the finest cell box spans $[-2 : +2]$ in each direction and the center of the source term is shifted to $(0.1, 0.09, 0.07)$ from the center to avoid the symmetry with respect to the cell configuration. The finest cell size is set to $1/12$. Thus, there are 48 cells in each direction in the finest cell box. For the sake of the interpolations, at least two (resp. three) coarse cell layers are added to both sides of the cell box in each direction in case of the second (resp. fourth) order discretization when the size of the coarser cell box is determined. 30 grid levels are made around the finest cell. In Fig. 6, the maximal solution errors on the outermost layer in the finest grid cells are plotted for various grid extension rates in case of the conservative discretizations. The error in the fourth order discretization drops more sharply than that of the second order discretization. The position of the error dropping in the fourth order case is shifted to the right from that of the second order case. These phenomena match well the estimates in (17) and (18). Note that the real grid extension rate approaches two as the cell box becomes coarser. This fact makes the change of accuracy gentler than what is expected from the theory.

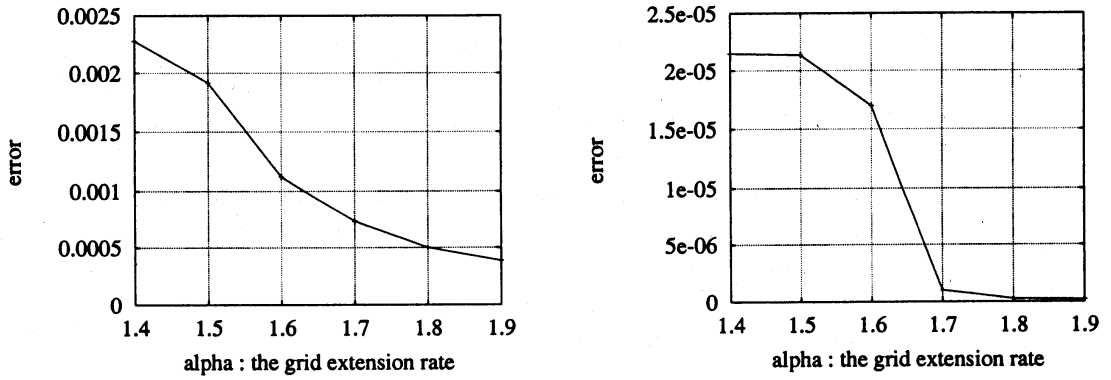

The second order conservative discretization

The fourth order conservative discretization

Figure 6: Maximum error on the outermost layer in the finest cell box for various grid extension rates in Problem 1.

Next, we compare the accuracy for the conservative and the non-conservative discretizations in the second and the fourth order approximation. For both problems, the center of the finest cell box is set at the origin. The finest cell box span $[-5 : +5]$ in each direction and the center of the source terms are shifted to $(1.9, 2.8, 1.3)$. To make the comparison fair, the grid extension rate is fixed to 1.8 for all cases and 30 grid levels are used. In Fig. 7, the maximum errors on the outermost layer in the finest box are plotted for $h = 5/8, 5/16, 5/32$. We see that excellent accuracy is attained with the Mehrstellen discretizations. In particular, the Mehrstellen shows better accuracy than the standard discretization even for the fairly coarse cell size in Problem 1, where the radius of the support of the source term is one. And we see that for the most cases the conservation improves the accuracy and it brings $O(h^2)$ and $O(h^4)$ behavior of the solution error.

Finally, we examine the convergence of the multigrid solution method. Here, we apply the multigrid V(1,1)-cycle, where one SOR relaxation with overrelaxation parameter 1.2 is applied as the pre- and post-smoothings. In the SOR relaxation, the red-black ordering is adopted for

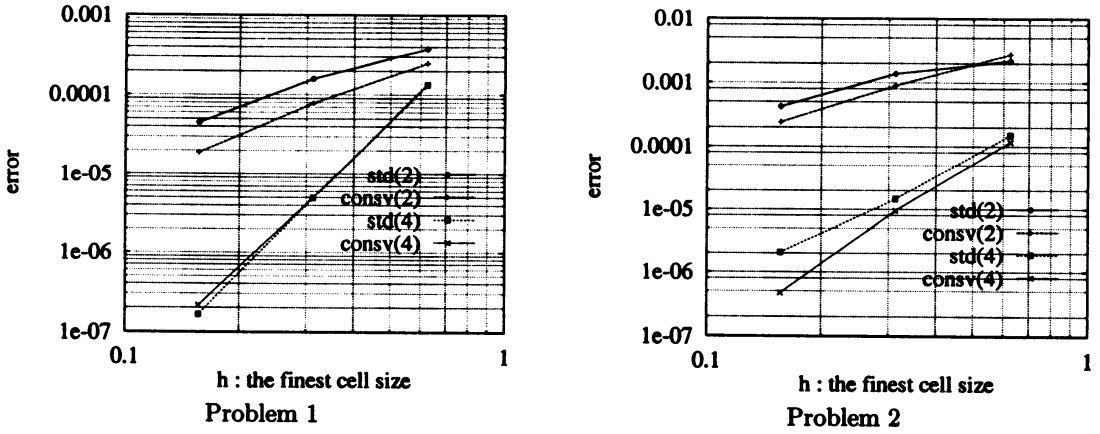

Figure 7: Maximum error on the outermost layer in the finest cell box. "std" indicates the solution from the standard MLAT and "consv" indicates the solution for the conservative discretization. The numbers of the brackets are the orders of the approximations.

the second order discretization, and the four color ordering[5] is adopted for the Mehrstellen discretization. The timing results are obtained on MIPS R10000 machine (200MHz). The experiments are performed under the same conditions as the previous one with 48 cells in each direction in the finest cell box. The grid extension rates are taken as $\alpha = 1.6$ for the second order and $\alpha = 1.8$ for the Mehrstellen. The cycle is terminated when the relative L_2 norm of the residual on the whole space is less than 10^{-10}. In Table 1, the CPU time in seconds and the number of cycles are given. The convergence of behaviors of the non-conservative (std) and the conservative schemes are similar. There are quite small overheads observed for the conservative scheme due to the additional work for the defect correction.

Table 1: Timing and convergence results for the standard discretization (std) and the conservative discretization (consv). The numbers of the brackets are the orders of the approximations.

Problem 1

discr.	time (s)	♯ iter
std(2)	9.02	10
consv(2)	9.55	10
std(4)	16.32	10
consv(4)	17.30	10

Problem 2

discr.	time (s)	♯ iter
std(2)	10.13	11
consv(2)	9.65	10
std(4)	16.87	10
consv(4)	18.21	10

8 Conclusion

In this paper, a conservative discretization scheme for cell centered finite volume discretizations of Poisson's equation on composite cells and its efficient solution method by multigrid were introduced. The conservation scheme was introduced not only to the standard second order discretization but also to the highly accurate Mehrstellen discretization. A way to construct the

composite cells around the source term to bound the solution error and the computational costs appropriately was given by the concept called the grid extension rate. Through the numerical experiments, it was shown that the proposed conservation technique improves the accuracy and is harmless to the computational cost of the solution method.

References

[1] D. Bai and A. Brandt, Local mesh refinement multilevel techniques, SIAM J. Sci. Stgat. Compute. 8, pp.109-134 (1987).

[2] T. L. Beck, Multigrid high order mesh refinement techniques for composite grid electrostatics calculations, J. Comp. Chem. 20, pp.1731–1739 (1999).

[3] A. Brandt, Multi-level adaptive solutions to boundary-value problems. Math. Comput. 31, pp.333–390 (1977).

[4] S. Fujino and T. Takeuchi, 3次元ポアソン方程式の右辺項の修正による高次精度の差分公式について, 日本応用数理学会論文誌, vol.15, No.1 pp.169–184 (1995).

[5] U. Trottenberg, C.W. Oosterlee and A. Shüller, MULTIGRID, Academic Press (2001).

[6] T.Washio and C.W. Oosterlee, Error analysis for a potential problem on locally refined grids, Numerische Mathematik, 86, pp.539–563 (2000).